Compact and Functional Co-Self-Assembled Monolayer for Efficient Inverted Wide-Bandgap Perovskite Solar Cells

Xinying Ruan, Jiahao Zhang, Xiaolong Liu, Wenli Shang, Yuechen Li, Xiaojun Li, Ye Zou, Ming-Hua Li, Chunru Wang and Fuwen Zhao**

1. General characterization

^{1}H and ^{13}C NMR spectra were measured on Bruker Avance-400 and Bruker Avance-600 spectrometers, respectively. UV-vis absorption spectra were measured on a UV-vis spectrophotometer (UV-2600i, Shimadzu, Japan). SEM was performed on Tescan Mira4. AFM was performed on a Bruker Dimension icon by using tapping mode. KPFM measurements were conducted by using a Bruker Dimension Icon with an AFM conducting tip. Standard AC mode imaging was employed for topography acquisition in the KPFM measurement. The contact angle was determined by using DSA30S KRUSS. X-ray photoelectron spectroscopy (XPS) and ultraviolet photoelectron spectroscopy (UPS) were detected by using a combined XPS/UPS system (Thermo Fisher Scientific, ESCALAB250XI), respectively. Steady-state photoluminescence (PL) was measured by Edinburgh Instruments (FLS980) at room temperature. Cyclic voltammetry (CV) was performed on an electrochemical workstation (CHI660C, Shanghai Chenhua Instrument Co., Ltd.). The measurement was recorded on a three-electrode system with tetra-*n*-butylammonium hexafluorophosphate (0.1 M) as the electrolyte in anhydrous acetonitrile under argon atmosphere. The glassy-carbon electrode, platinum-wire, and Ag/AgCl electrode were used as working, counter, and reference electrodes, respectively. Both samples were deposited on the glassy-carbon electrode. All potentials were corrected against Fc/Fc^{+}. Transient photovoltage (TPV) and transient photocurrent (TPC) measurements were performed on an all-in-one characterization platform Paios developed by Fluxim AG. The *J-V* curves were measured by using a Keithley 2450 source-measure unit in the nitrogen-filled glove box along the reverse scan direction from -0.1 V to 1.4 V at room temperature. The scan speed and dwell times were fixed at 0.02 V per step and 0 ms, respectively. The photocurrent was measured under AM 1.5G illumination at 100 mW cm^{-2} by using a 3A solar simulator (LSS-55, Lightsky Technology Co., Ltd). Light intensity was calibrated with a standard photovoltaic cell equipped with a KG5 filter (certificated by the National Institute of Metrology). The EQE measurements of devices were carried out in the air with a solar cell spectral response measurement system (LST-QE, Lightsky Technology Co., Ltd). The light intensity at each wavelength was calibrated by a standard single-crystal Si photovoltaic cell. The thickness of all films was measured by the Bruker Dektak-XT. The energy level of the frontier molecular orbitals as well as the dipole moment for the SAMs were calculated with the Gaussian 16 c.01 package.[1] The calculations were conducted using B3LYP functional and a 6-31G(d,p) basis set. The Grimme's D3-correction with Becke-Johnson damping (GD3BJ) was used for dispersion correction.[2]

2. Synthesis

Unless stated otherwise, all solvents and chemical reagents were obtained commercially and used without further purification. 9*H*-carbazole-3-carbonitrile was prepared, according to the literature.[3]

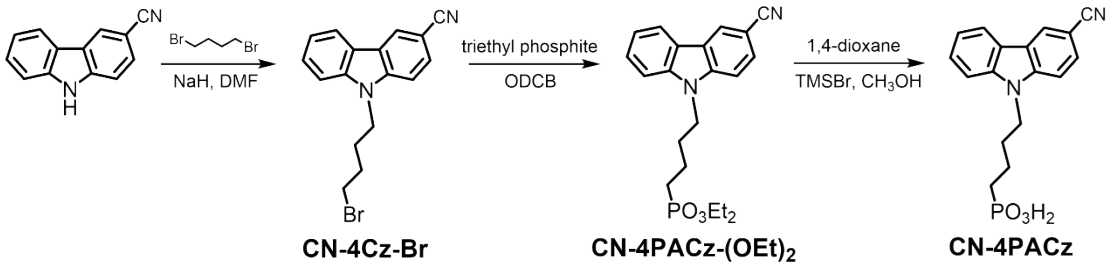

Scheme S1. Synthetic route of CN-4PACz.

CN-4Cz-Br. 9*H*-carbazole-3-carbonitrile (100 mg, 0.52 mmol) was dissolved in 30 mL DMF. Sodium hydride (25 mg, 1.04 mmol) was added to the solution, and the mixture was stirred at 0 °C for 1 hour. Subsequently, 1,4-dibromobutane (138.4 mg, 0.78 mmol) was added. The reaction mixture was warmed up to room temperature and stirred for an additional 2 hours. Upon completion of the reaction, the mixture was quenched with ice water, followed by the suction filtration to afford CN-4Cz-Br (145 mg, 85%). ^{1}H NMR (400 MHz, $CDCl_3$) δ: 8.40 (d, *J* = 1.1 Hz, 1H), 8.11 (d, *J* = 7.8 Hz, 1H), 7.71 (dd, *J* = 8.5, 1.6 Hz, 1H), 7.56 (ddd, *J* = 8.3, 7.2, 1.1 Hz, 1H), 7.46 (dd, *J* = 8.4, 5.7 Hz, 2H), 7.38-7.31 (m, 1H), 4.39 (t, *J* = 7.1 Hz, 2H), 3.40 (t, *J* = 6.4 Hz, 2H), 2.18-2.01 (m, 2H), 1.99-1.84 (m, 2H).

CN-4PACz-$(OEt)_2$. CN-4Cz-Br (150 mg, 0.46 mmol) was dissolved in 50 mL *o*-dichlorobenzene. Triethyl phosphite (152.72 mg, 0.92 mmol) was added to the solution. The mixture was stirred for 24 hours. After the completion of the reaction, *o*-dichlorobenzene and excess triethyl phosphite were removed via reduced pressure distillation. The crude product was purified via column chromatography on silica gel by using acetone/petroleum ether (1:1) as the eluent to afford CN-4PACz-$(OEt)_2$ (160 mg, 90%). ^{1}H NMR (400 MHz, $CDCl_3$) δ: 8.39 (d, *J* = 1.1 Hz, 1H), 8.10 (d, *J* = 7.8 Hz, 1H), 7.70 (dd, *J* = 8.5, 1.5 Hz, 1H), 7.54 (dd, *J* = 11.3, 4.1 Hz, 1H), 7.44 (dd, *J* = 8.4, 3.9 Hz, 2H), 7.32 (t, *J* = 7.5 Hz, 1H), 4.35 (t, *J* = 7.1 Hz, 2H), 4.10-3.96 (m, 4H), 2.06-1.94 (m, 2H), 1.72-1.63 (m, 4H), 1.25 (t, *J* = 7.1 Hz, 6H).

CN-4PACz. CN-4PACz-$(OEt)_2$ (160 mg, 0.41 mmol) was dissolved in 50 mL 1,4-dioxane. Trimethylsilyl bromide (191 mg, 1.25 mmol) was added to the resulting solution. The mixture was stirred for 48 hours. Methanol was then introduced. The mixture was stirred for an additional 3 hours, followed by the addition of deionized water with stirring for 15 hours. Upon completion of the reaction, methanol was added dropwise to the mixture, which was further stirred for 3 hours. Subsequently, deionized water was added until the reaction mixture became turbid. The mixture was stirred overnight. Finally, the solid, obtained by suction filtration, was washed sequentially with water and diethyl ether, and dried to afford CN-4PACz (104 mg, 77%). ^{1}H NMR (400 MHz, DMSO) δ: 8.74 (s, 1H), 8.28 (d, *J* = 7.7 Hz, 1H), 7.82 (s, 2H), 7.73 (d, *J* =

8.3 Hz, 1H), 7.63-7.49 (m, 1H), 7.30 (t, *J* = 7.5 Hz, 1H), 4.47 (t, *J* = 7.1 Hz, 2H), 1.96-1.77 (m, 2H), 1.53 (dd, *J* = 12.9, 4.0 Hz, 4H). ^{13}C NMR (151 MHz, DMSO) δ: 141.75, 140.59, 128.72, 127.10, 125.49, 122.26, 121.30, 121.02, 120.48, 120.10, 110.50, 110.08, 100.34, 42.29, 29.36, 26.76, 20.34. HRMS-ESI (m/z): 327.09030 $[M\text{-}H^+]^-$, calcd. for $C_{17}H_{16}N_2O_3P$ (327.08985).

3. NMR spectra

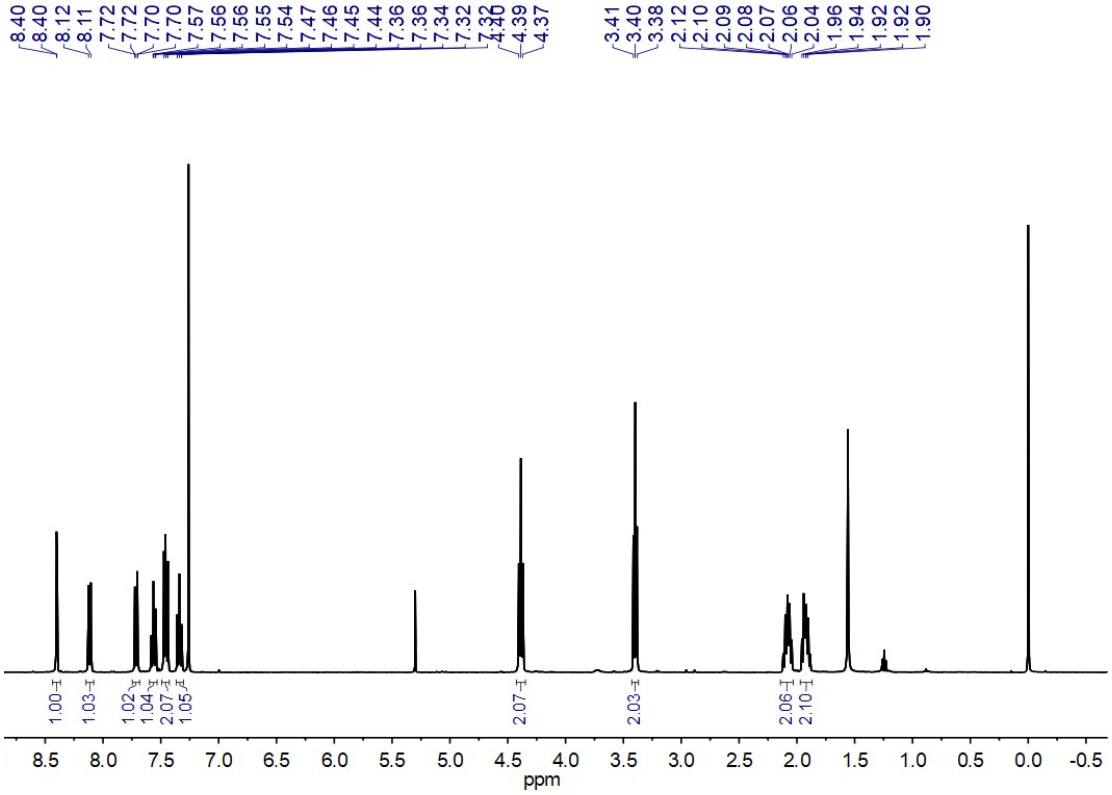

Fig. S1 ^{1}H NMR spectrum of CN-4Cz-Br in $CDCl_3$.

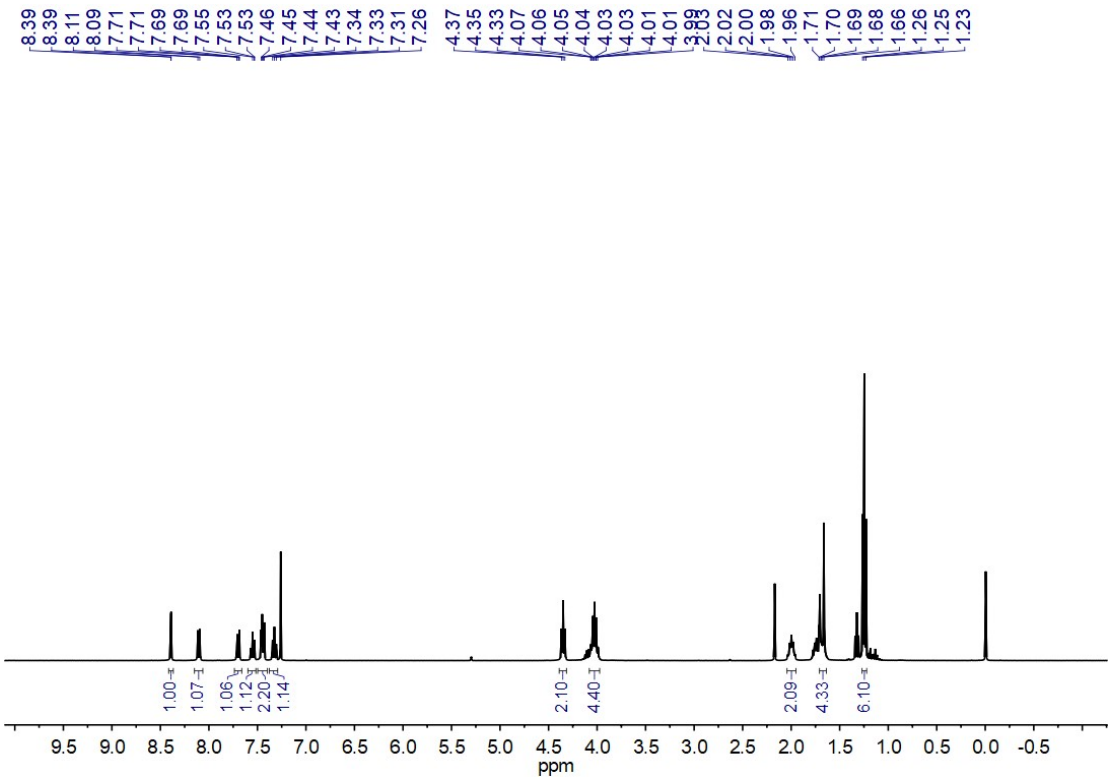

Fig. S2 ^{1}H NMR spectrum of CN-4PACz-$(OEt)_2$ in $CDCl_3$.

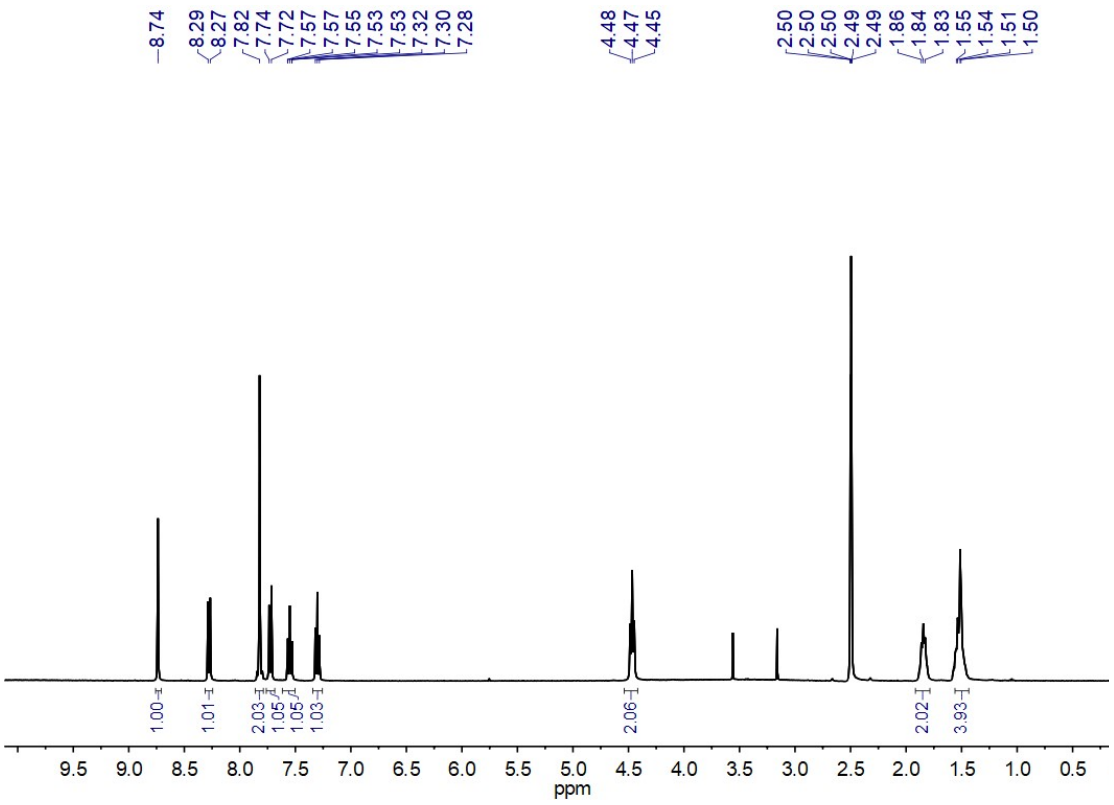

Fig. S3 ^{1}H NMR spectrum of CN-4PACz in DMSO-d_6.

4. Mass spectrum

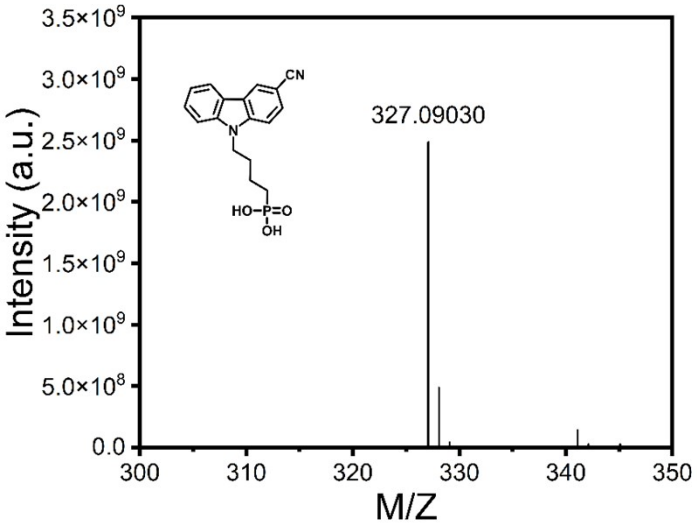

Fig. S4 High-resolution mass spectrum of CN-4PACz.

5. Device fabrication and measurement

The pre-patterned FTO substrates were ultrasonically cleaned with detergent, deionized water, and ethanol for 15 min, successively. Then the FTO glass substrates were dried with nitrogen flow and cleaned by ultraviolet ozone for 15 min, and then transferred into a nitrogen-filled glovebox for further device fabrication. Me-4PACz or co-SAM (Me-4PACz:CN-4PACz = 2:1 (w/w), the total concentration was 0.5 mg ml^{-1} in ethanol) was deposited onto the FTO substrates via spin-coating at 3000 rpm for 30 s, followed by annealing on a hot table at 100 °C for 10 min in a nitrogen-filled glove box. The 1.2 M WBG perovskite $FA_{0.75}Cs_{0.25}Pb(I_{0.5}Br_{0.5})_3$ precursor was prepared via dissolving 0.9 mmol FAI, 0.3 mmol CsI, 0.3 mmol PbI_2, 0.9 mmol $PbBr_2$, and 0.012 mmol $Pb(SCN)_2$ in a mixed solvent of DMF and DMSO with a volume ratio of 4:1 and stirred for 3 h. To deposit the perovskite layer, 100 μL perovskite precursor was dropped on the substrate and quickly spin-coated by using a two-stage technique (500 rpm for 2 s and 4000 rpm for 60 s), with 300 μL chlorobenzene (CB) dripped at 30 s of the second step. Then the as-prepared perovskite film was annealed at 100 °C for 5 min. After the perovskite films were cooled down to room temperature, PDADI (1,3-diaminopropane dihydroiodide) (1 mg mL^{-1} in IPA) was spin-coated onto the perovskite surface at 3000 rpm for 30 s and annealed at 100 °C for 5 min. After cooling down to room temperature, the electron transport layer (ETL) was obtained via spin-coating the $PC_{61}BM$ solution (20 mg mL^{-1} in CB) on the substrate at 3000 rpm for 30 s. Then, it was spin-coated with BCP (0.5 mg mL^{-1} in IPA) at 5000 rpm for 30 s. Finally, all samples were transferred into the multi-source evaporation chamber and ~100 nm Ag was evaporated at 5×10^{-4} Pa. The active areas of the devices through an aperture mask are 0.09 cm^2.

6. Energy level calculation

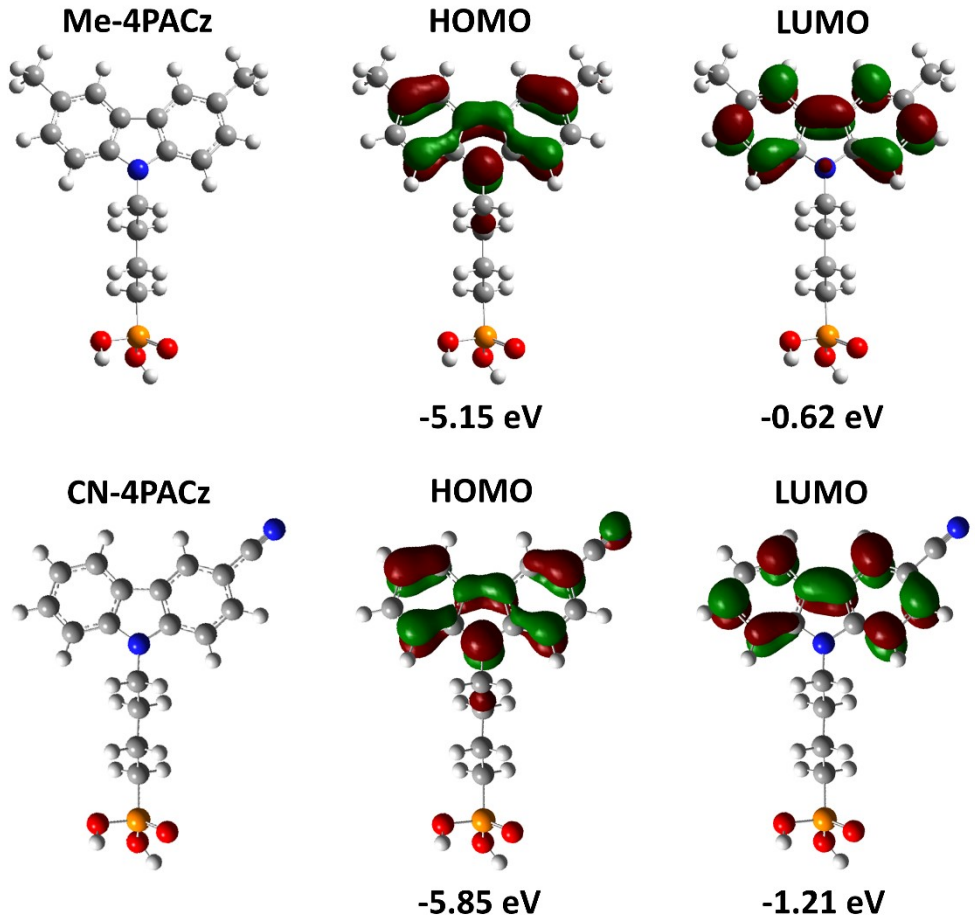

Fig. S5 Optimized chemical structures, HOMO and LUMO energy levels of Me-4PACz and CN-4PACz.

7. CV

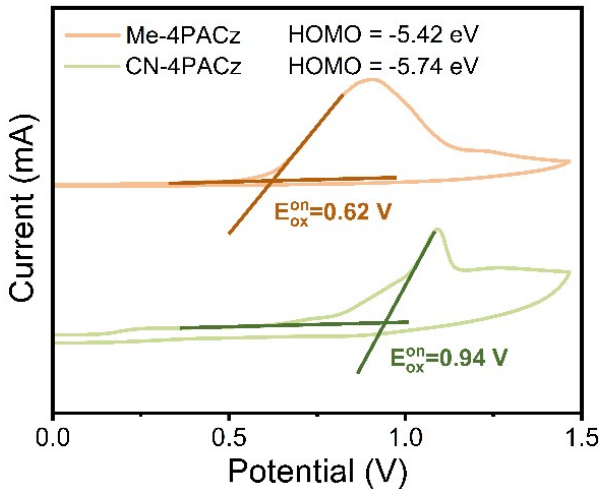

Fig. S6 CV curves of Me-PACz and CN-4PACz. HOMO = -(E_{ox}^{on} +4.8).

8. UPS

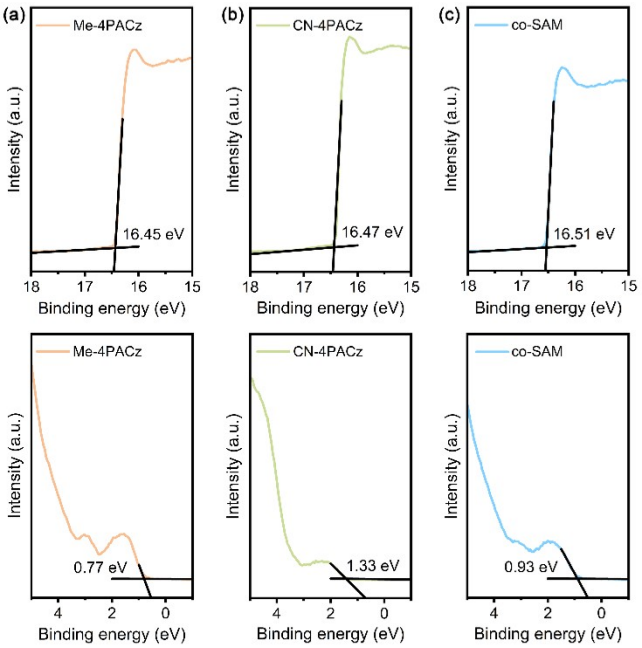

Fig. S7 Cutoff regions and valence band edges of UPS spectra for (a) Me-4PACz, (b) CN-4PACz and (c) co-SAM.

Table S1. Electronic structure parameters from UPS.

Sample	E_{cutoff} (eV)	E_{VB}^{F} (eV)	Φ (eV)	IP (eV)	E_{HOMO} (eV)
Me-4PACz	16.45	0.77	4.77	5.54	-5.54
CN-4PACz	16.47	1.33	4.75	6.08	-6.08
co-SAM	16.51	0.93	4.71	5.64	-5.64

Notes: E_{cutoff} value is the kinetic energy of the secondary electron cutoff. E_{VB}^{F} is the valence band maximum energy relative to the vacuum level. The work function is calculated as $\Phi = h\nu - E_{\text{cutoff}}$, where $h\nu$ is the photon energy. The ionization potential is calculated as IP = $\Phi + E_{VB}^{F} = h\nu - E_{\text{cutoff}} + E_{VB}^{F}$. The energy of HOMO level relative to the vacuum level is determined by: E_{HOMO} = -IP = -($\Phi + E_{VB}^{F}$) = –($h\nu - E_{\text{cutoff}} + E_{VB}^{F}$).

9. XPS

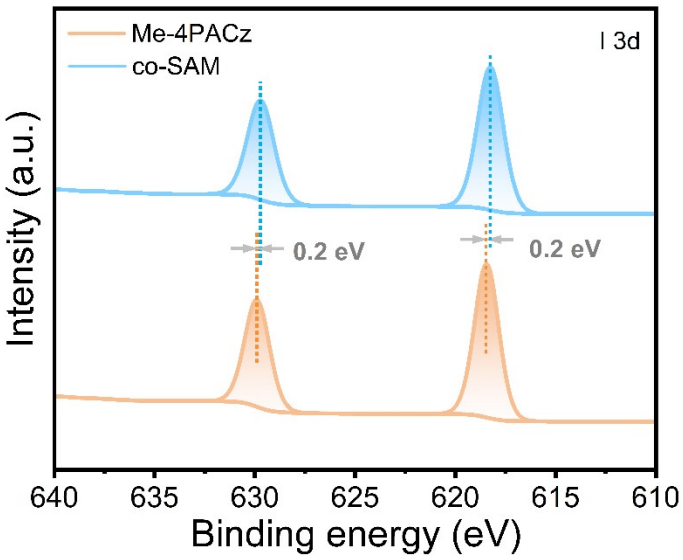

Fig. S8 XPS spectra for I 3d of the bottom surface of perovskite films deposited on Me-4PACz and co-SAM.

10. FT-IR spectroscopy

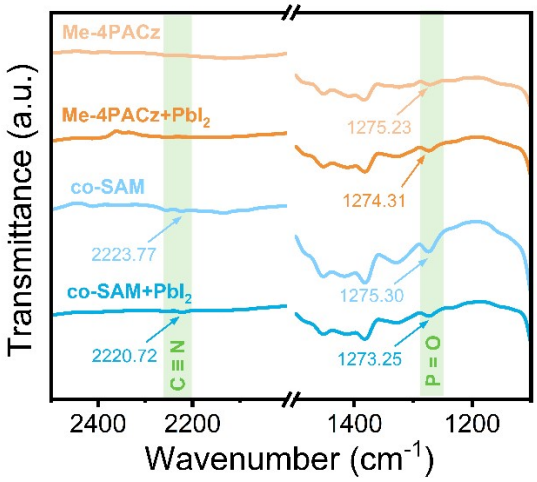

Fig. S9 FT-IR spectroscopy for Me-4PACz, co-SAM, Me-4PACz+PbI_2 and co-SAM+ PbI_2.

11. Contact angles

Contact angles of water and glycerol on Me-4PACz and co-SAM were measured by DSA30S KRUSS contact angle analyzer. The surface tension can be evaluated by using the equation[4]:

$$\gamma_{LV}(1+cos\theta) = 4\frac{\gamma_S^d\gamma_L^d}{\gamma_S^d+\gamma_L^d} + 4\frac{\gamma_S^p\gamma_L^p}{\gamma_S^p+\gamma_L^p}$$

where γ_{LV} represents the surface tension of water/glycerol in equilibrium with its vapor.

γ_L^d and γ_L^p represent the dispersion and polar components of the liquid surface tension, respectively, while γ_S^d and γ_S^p represent the dispersion and polar components of the solid surface tension, respectively. γ_S^d and γ_S^p can be calculated by using the contact angles with water and glycerol. The surface tension of donor and acceptors are calculated by equation: $\gamma = \gamma_S^d + \gamma_S^p$.

Table S2. Contact angle and surface energy parameters.

Surface	θ_{water} (°)	$\theta_{glycerol}$ (°)	γ_S^d (mN m^{-1})	γ_S^p (mN m^{-1})	γ (mN m^{-1})
Me-4PACz	91.3	84.8	11.05	13.15	24.20
co-SAM	85.3	81.2	10.02	17.14	27.16

12. Electrical conductivity

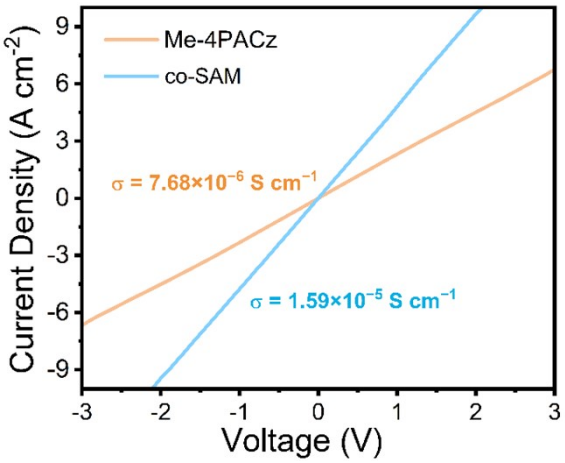

Fig. S10 *I-V* characteristics of electrical conductivity of devices with the structure of FTO/Me-4PACz or co-SAM/Ag.

13. AFM measurement

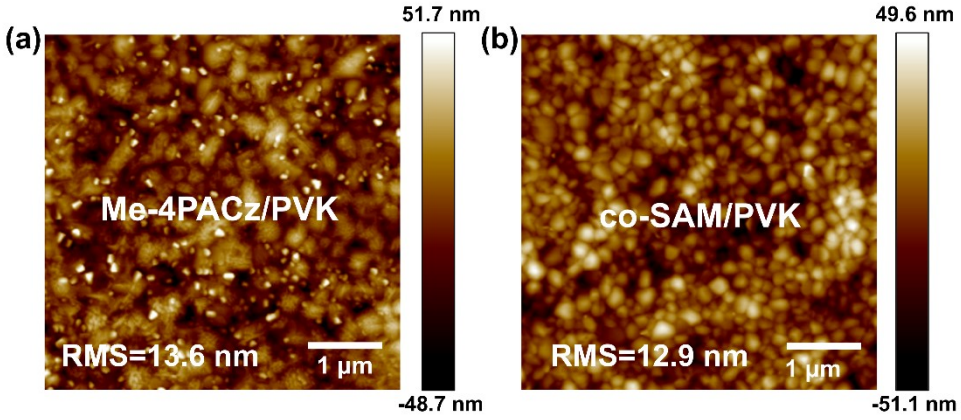

Fig. S11 AFM height images of (a) Me-4PACz/PVK and (b) co-SAM/PVK films.

14. PL

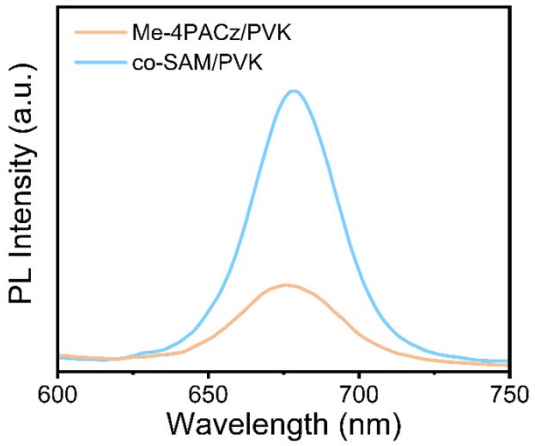

Fig. S12 PL of the perovskite films deposited on Me-4PACz and co-SAM.

15. EQE measurement

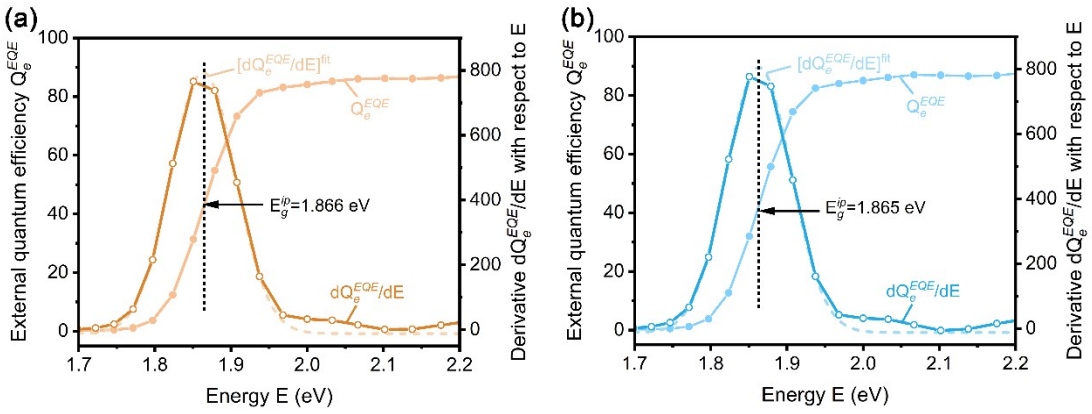

Fig. S13 EQE spectra, corresponding derivatives dQ_e^{EQE}/dE versus E and calculated E_g^{ip} values of devices with (a) Me-4PACz and (b) co-SAM.

Note: There are several definitions of bandgap used for perovskite solar cells in the literatures. We used this standardized approach to evaluate the bandgap of perovskite solar cells in this paper. After digitizing the external quantum efficiency Q_e^{EQE} of the

solar cell, we calculated the derivative of $\mathrm{d}Q_e^{EQE}/\mathrm{d}E$ following with a corresponding Gauss fitting. The maximum of the derivative is properly regarded as the inflection point E_g^{ip}, which is generally at the band edge of the Q_e^{EQE}.[5,6]

16. Photovoltaic parameters

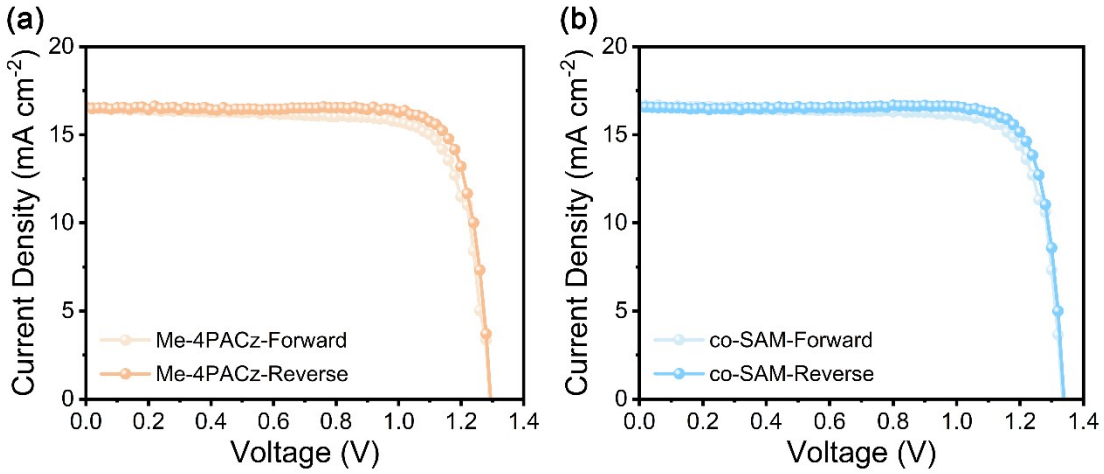

Fig. S14 Current density-voltage (*J-V*) curves with forward and reverse scans of PSCs based on (a) Me-4PACz and (b) co-SAM.

Table S3. Photovoltaic parameters of best-performing PSCs based on Me-4PACz and co-SAM as HTLs.

		J_{SC} (mA cm^2)	V_{OC} (V)	FF (%)	PCE (%)	Integrated J_{SC} (mA cm^2)	Hysteresis factor
Me-4PACz	Reverse	16.517	1.295	81.62	17.45	15.73	5.3%
	Forward	16.577	1.291	77.20	16.52		
co-SAM	Reverse	16.554	1.339	83.08	18.41	15.82	3.5%
	Forward	16.658	1.335	79.88	17.76		

Notes: A consistency check between EQE measurement and *J-V* characterization was performed. The photocurrent density derived from EQE spectra, denoted as integrated J_{SC}, was calculated via the integration of EQE response over the AM1.5G solar spectrum. The value was compared with the short-circuit current density (J_{SC}) obtained from the reverse voltage scan direction of *J-V* curves. The reverse scan data are referenced for this comparison, since it typically exhibits reduced transient hysteresis artifacts. The relative deviation is found to be within 5% for all champion devices. The high consistency substantiates the fidelity of the photocurrent values we reported. The hysteresis factor is calculated as HF = $PCE_{reverse}$-$PCE_{forward}$/$PCE_{reverse}$.[7]

17. SOP curves

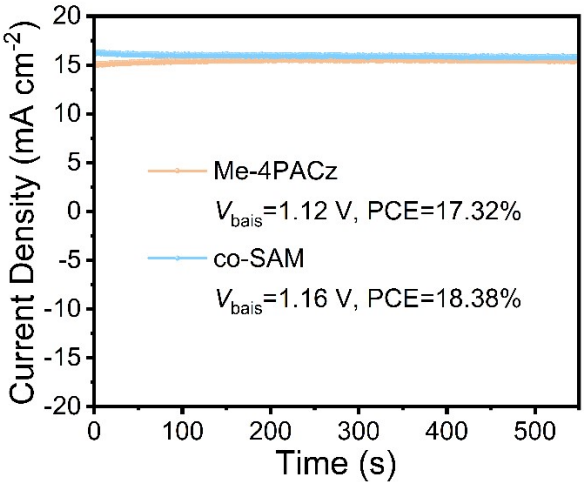

Fig. S15 Steady-state output power curves of PSCs with Me-4PACz and co-SAM as hole transport layers.

18. Photovoltaic parameter distribution

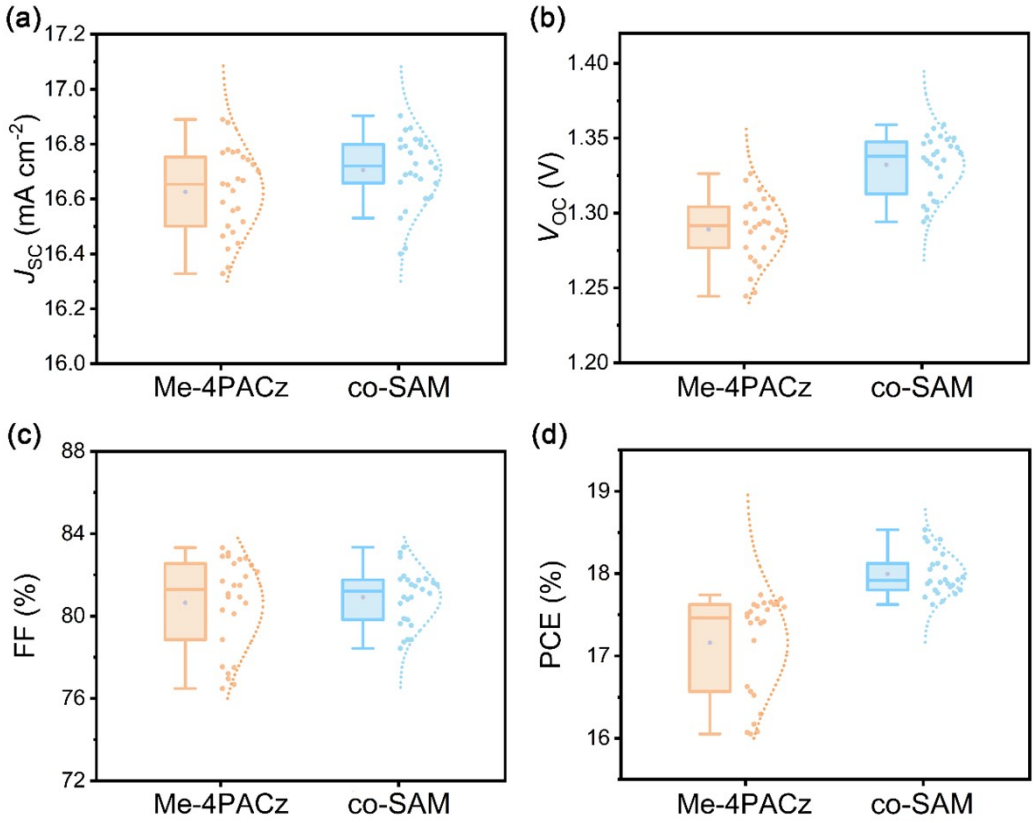

Fig. S16 Statistical photovoltaic parameters of (a) J_{SC}, (b) V_{OC}, (c) FF and (d) PCE for independent PSCs based on Me-4PACz and co-SAM obtained from the reverse voltage scan direction.

Table S4. Summary of photovoltaic parameters for PSCs based on Me-4PACz and co-SAM as HTLs.

		J_{SC} (mA cm^2)	V_{OC} (V)	FF (%)	PCE (%)
Me-4PACz	Reverse	16.469±0.620	1.295±0.019	81.70±2.72	17.41±1.10
	Forward	16.734±0.479	1.279±0.027	73.58±3.13	15.74±0.84
co-SAM	Reverse	16.724±0.141	1.338±0.018	81.54±0.67	18.24±0.21
	Forward	16.900±0.190	1.333±0.024	77.27±3.18	17.41±0.86

The values represent the average ± standard deviation from 10 independent devices for each SAM.

19. Dark *J-V* curves

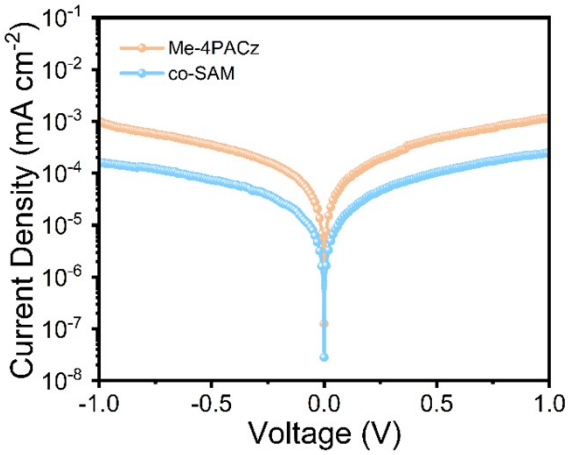

Fig. S17 Dark *J-V* curves of devices based on Me-4PACz and co-SAM.

20. EIS

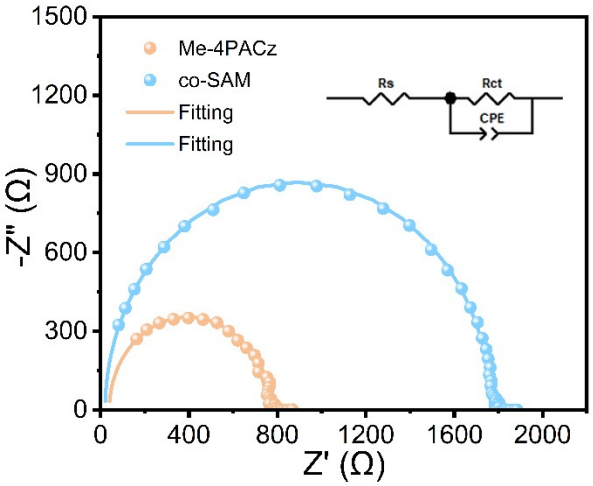

Fig. S18 Electrochemical impedance spectra (EIS) of devices based on Me-4PACz and co-SAM (The inset is the equivalent circuit.), where R_S is the series resistance, R_{ct} is the charge recombination resistance, and the fitting results are expressed with solid lines in the Nyquist plots.

Table S5. EIS fitting parameters for Me-4PACz and co-SAM-based devices.

	R_S (Ω cm^2)	R_{ct} (Ω cm^2)	CPE-T (S s$^{\alpha-1}$)	CPE-P
Me-4PACz	38.96	713	4.887×10^{-9}	0.99871
co-SAM	20.38	1745	4.836×10^{-9}	0.99726

References

[1] Gaussian 16, Revision C.01, M. J. Frisch, G. W. Trucks, H. B. Schlegel, G. E. Scuseria, M. A. Robb, J. R. Cheeseman, G. Scalmani, V. Barone, G. A. Petersson, H. Nakatsuji, X. Li, M. Caricato, A. V. Marenich, J. Bloino, B. G. Janesko, R. Gomperts, B. Mennucci, H. P. Hratchian, J. V. Ortiz, A. F. Izmaylov, J. L. Sonnenberg, D. Williams-Young, F. Ding, F. Lipparini, F. Egidi, J. Goings, B. Peng, A. Petrone, T. Henderson, D. Ranasinghe, V. G. Zakrzewski, J. Gao, N. Rega, G. Zheng, W. Liang, M. Hada, M. Ehara, K. Toyota, R. Fukuda, J. Hasegawa, M. Ishida, T. Nakajima, Y. Honda, O. Kitao, H. Nakai, T. Vreven, K. Throssell, J. A. Montgomery, Jr., J. E. Peralta, F. Ogliaro, M. J. Bearpark, J. J. Heyd, E. N. Brothers, K. N. Kudin, V. N. Staroverov, T. A. Keith, R. Kobayashi, J. Normand, K. Raghavachari, A. P. Rendell, J. C. Burant, S. S. Iyengar, J. Tomasi, M. Cossi, J. M. Millam, M. Klene, C. Adamo, R. Cammi, J. W. Ochterski, R. L. Martin, K. Morokuma, O. Farkas, J. B. Foresman, and D. J. Fox, Gaussian, Inc., Wallingford CT, 2019.

[2] S. Grimme, S. Ehrlich and L. Goerigk, *J. Comput. Chem.*, 2011, **32**, 1456-1465.

[3] T. Shirisha, S. Majhi and D. Kashinath, *ChemistrySelect*, 2024, **9**, e202401275.

[4] Ghoufi, *Nat. Rev. Phys.*, 2025, **7**, 473-486.

[5] L. Krückemeier, U. Rau, M. Stolterfoht and T. Kirchartz, *Adv. Energy Mater.*, 2020, **10**, 1902573.

[6] Y. Yuan, G. Yan, R. Hong, Z. Liang and T. Kirchartz, *Adv. Mater.*, 2022, **34**, 2108132.

[7] L. Zhang, M. Fu, X. Jiang, Z. Zhang, C. Wang, Z. Su, B. He, L. Tang, G. Zheng, X. Gao and J. He, *Adv. Sci.*, 2025, **12**, e12117.